

## Renormalized Random Walk Study of Oxygen Absorption in the Human Lung

M. Felici,<sup>1</sup> M. Filoche,<sup>1,2</sup> and B. Sapoval<sup>1,2</sup>

<sup>1</sup>Laboratoire de Physique de la Matière Condensée, Ecole Polytechnique C.N.R.S., 91128 Palaiseau, France

<sup>2</sup>Centre de Mathématiques et leurs Applications, ENS Cachan, 94235 Cachan, France

(Received 23 April 2003; published 12 February 2004)

The possibility to renormalize random walks is used to study numerically the oxygen diffusion and permeation in the acinus, the diffusion cell terminating the mammalian airway tree. This is done in a 3D tree structure which can be studied from its topology *only*. The method is applied to the human acinus real morphology as studied by Haefeli-Bleuer and Weibel in order to compute the respiratory efficiency of the human lung. It provides the first quantitative evidence of the role of diffusion screening in real 3D mammalian respiration. The net result of this study is that, at rest, the efficiency of the human acinus is only of order 33%. Application of these results to CO<sub>2</sub> clearance provides for the first time a theoretical support to the empirical relation between the O<sub>2</sub> and CO<sub>2</sub> partial pressures in blood.

DOI: 10.1103/PhysRevLett.92.068101

PACS numbers: 87.10.+e, 05.60.-k, 87.19.-j

Gas exchange in the peripheral airways of the human lung is obviously a major process for respiration. For physicists, this is a diffusion-reaction problem in an irregular space-filling structure in 3D [1]. But up to now, physiologists, with the lack of any means to really examine this question, have postulated that diffusion was sufficiently fast to create a uniform oxygen partial pressure distribution. In particular, the importance of partial pressure gradients is not known in current respiratory physiology, the only data available being the mean partial pressures over the whole lung [2]. On the other hand, recent polarized gases magnetic resonance imaging (MRI) studies have given some information on gas diffusion at smaller scales [3]. To interpret this kind of data, a deeper knowledge of the diffusion processes in this complex system is needed. A new insight to this problem can come from theoretical studies on the physics of diffusion towards and across irregular surfaces [4]. The challenge is then to solve the diffusion-reaction problem for oxygen in a realistic, or even real, geometry. This is the physical problem which is solved here.

In the human lung, the airway tree is a dichotomous branched structure counting 23 generations of ducts [2]. The first 17 generations constitute the bronchial tree distributing the air flow. In the last six generations, alveoli appear on the duct walls. The alveolated ducts originating from the same nonalveolated duct form an ensemble called the *pulmonary acinus* [shown, from outside, in Fig. 1(a)]. The acinus is the gas exchange unit where oxygen is transferred into blood through the alveolar membrane. The global transfer of oxygen is then achieved through three successive steps: ventilation in the conducting airways, diffusion of oxygen in quasistatic air to the alveolar surface, and final diffusion of oxygen across the alveolar membrane into capillary blood [2]. We focus here on the oxygen diffusional transfer in the acinus. The direct numerical simulation of this process is not possible because of the complicated 3D geometry. This Letter shows that a convenient renormalization of the diffusion

random walks permits one to solve the oxygen transfer problem, using *only* the acinus topology [see Fig. 1(b)].

The mathematical model describing the acinus functioning at rest is sketched in Fig. 2. A fixed concentration  $C_0$  is set at the entry. As alveoli cover the acinar duct walls, the absorbing interface is the entire system boundary. In steady state, the oxygen concentration  $C$  obeys the Laplace equation,  $\nabla^2 C = 0$ , with mixed boundary conditions:  $\frac{\partial C}{\partial n} = \frac{1}{\Lambda} C$ . This finite absorption condition is imposed by the conservation of the oxygen flux  $J$  across the interface. In the bulk,  $J$  obeys Fick's law  $\vec{J} = -D\nabla C$ , whereas at the interface  $J_n = -WC$ , where  $n$  is the in-normal to the surface,  $D$  the diffusion coefficient of oxygen in air, and  $W$  the permeability of the membrane. The permeability is defined as the flux per unit area and per unit concentration difference between the two sides of the

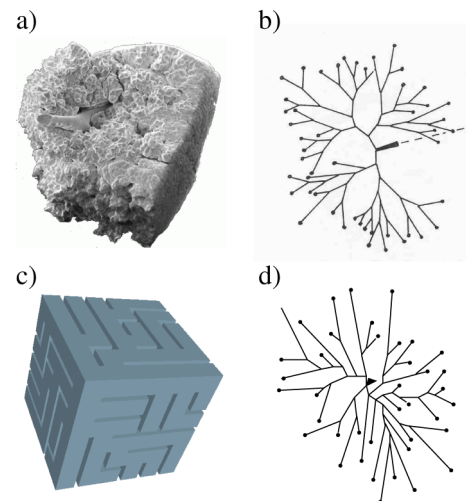


FIG. 1 (color online). (a) Silicon cast of a human acinus (8 subacini); (b) graph of the topological structure of a human subacinus [1]; (c) 3D Kitaoka geometry corresponding to a human subacinus; and (d) graph of the topological structure of Kitaoka geometry shown in (c).

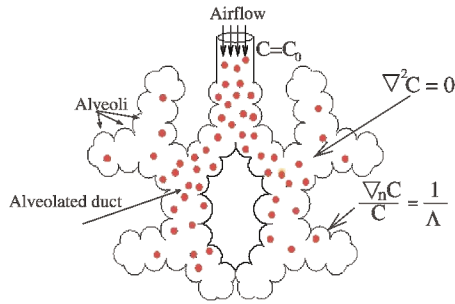


FIG. 2 (color). Schematic representation of how the acinus works at rest. The arrow ends stand for the convection-diffusion transition; oxygen is depicted in red.

membrane. The value  $\Lambda \equiv \frac{D}{W}$  results from flux conservation. In this first approach, the oxygen concentration in blood is set to a constant value [5,6]. Note that the equations for the concentration are linear and hold both for oxygen uptake (with a source at the entry) and  $\text{CO}_2$  clearance (with the source at the membrane surface).

The length  $\Lambda$ , is called the *unscreened perimeter length* [4], as it gives a typical value for the perimeter of the portion of the absorbing surface over which diffusion screening can be neglected. To understand the role of  $\Lambda$ , one can compare the conductance to reach an irregular surface of area  $A_T$  and diameter  $L_A$  with the conductance to cross this surface (the diameter of a surface is the diameter of the smallest sphere that surrounds the surface). The conductance to reach the surface is of order  $Y_{\text{reach}} \sim DL_A$ , whereas the conductance to cross is  $Y_{\text{cross}} = WA_T$ . If the membrane permeability is small enough, the conductance to reach is larger than the conductance to cross  $Y_{\text{reach}} > Y_{\text{cross}}$  and the surface works uniformly. For given  $D$  and  $W$ , a situation where  $Y_{\text{reach}} < Y_{\text{cross}}$  is reached for a large enough system. In this case, the less accessible regions are submitted to screening. The transition between the screened and unscreened regimes is determined by  $Y_{\text{cross}} \sim Y_{\text{reach}}$ . It occurs when  $\Lambda (=D/W)$  is close to  $A_T/L_A \equiv L_p$ . The length  $L_p$  roughly corresponds to the average total perimeter of a random plane section of the surface [5]. It has been shown recently that the perimeter of the pulmonary acini in several mammals is of order  $\Lambda$ , indicating that screening plays a role in oxygen uptake [5].

Up to now, our knowledge was based on 2D analogies, but a good quantitative estimate of this effect in realistic 3D acini is important to reach, as a change by a factor of 2 in the oxygen supply is known to induce serious health hazards. We are then interested in computing how the acinus works as a gas exchanger. More precisely, one defines the acinus *efficiency*  $\eta$  as

$$\eta = \frac{\int WCdS}{WC_0S}, \quad (1)$$

where  $S$  is the absorbing surface area. Equation (1) states that  $\eta$  is the ratio of the total flux across the surface to the

total flux in the ideal condition of infinite diffusivity (but finite permeability). The efficiency then measures the fraction of the acinar surface that is active for respiration. In a lung containing  $N_{\text{ac}}$  acini, the total oxygen uptake  $\Phi_{\text{tot}}$  can be written as

$$\Phi_{\text{tot}} = N_{\text{ac}} WC_0 S \cdot \eta. \quad (2)$$

One has then to solve numerically the diffusion equation for the oxygen concentration. Unfortunately, exact maps of the alveolar surface in 3D are not available. Moreover, even if the 3D structure were known, a direct numerical approach would not be possible due to the size of the system, which possesses about 1000 alveoli. The morphometric studies on silicon casts, as the one in Fig. 1(a), have yielded the branching structure and the acinar ducts sizes. In Fig. 1(b) the graph of the intracinar pathways (topology) of a real human acinus [1] is shown. In the following, we use a coarse-graining procedure that allows one to map the 3D continuous problem stated above into the study of a discretized random walk on the tree designed on the acinus topological structure. As there exists so far no exact mapping, one has to test the procedure in a case where a complete numerical solution is possible. For this, we use a branched geometry for which *both* topology and the entire 3D structure are known. The model acinus used for this comparison has been introduced by Kitaoka [7]. Its geometry results from a semistochastic algorithm that constructs labyrinths, filling a cube of side  $L$ , made of  $L^3$  unit cubic cells, one corner being chosen as the entry. Although apparently artificial, this model presents the same type of topological complexity as the real acini. Each cell, with side  $\ell = 0.5$  mm, comprises eight alveoli. With  $L/\ell = 6$ , the number of branchings, the mean branch length, and the number of alveoli are close to those of a human subacinus [1,5]. A Kitaoka geometry with  $6 \times 6 \times 6$  cells is shown in Fig. 1(c) and its topological structure in Fig. 1(d).

As the real acinus, the  $6 \times 6 \times 6$  model acinus is too large to be solved directly. However, for a smaller Kitaoka 3D structure, a computation of the continuous problem with sufficiently refined meshes is possible. Figure 3 shows the oxygen concentration distribution in the  $4 \times 4 \times 4$  acinus as computed using a 3D finite elements (FEM) solver for  $\Lambda/\ell = 256$ . The efficiency has been computed for  $3 \times 3 \times 3$  and  $4 \times 4 \times 4$  acini and is given in Fig. 4 (full symbols). As one can see,  $\eta$  increases as a power law for small values of  $\Lambda$  and then approaches 1. For the same value of  $\Lambda$ , smaller acini are more efficient [5,6].

The idea of the random walks (RW) approach is to take advantage of the scale invariance of the RW in free space. Here, it means that diffusion walks can be renormalized up to a size of the order of an alveolus or duct diameter. Consequently, the complete partial differential equations (PDE) solution can be replaced by the study of RW on the skeleton of the acinus. A branching lattice is designed,

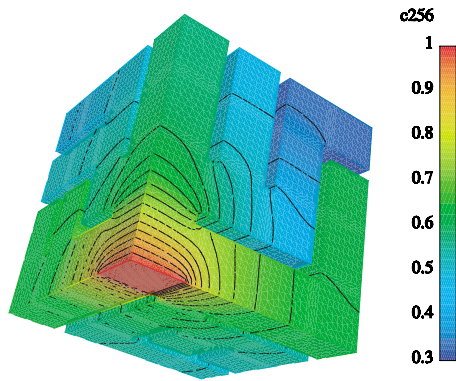


FIG. 3 (color). Distribution of the oxygen concentration (or partial pressure) in a  $4 \times 4 \times 4$  Kitaoka model acinus for  $\Lambda/\ell = 256$ .

where each  $1d$  branch represents an alveolar duct and has one site per unit distance  $\ell$ ,  $\ell$  being the duct diameter. Molecular diffusion is simulated by a superposition of random walks on the lattice, starting at the entry. To represent the absorption on the ducts walls, one has to introduce in a proper way an absorption probability  $\sigma$  for the walkers. For that purpose, one defines the coordination number  $n_i$  as the number of neighbors of the site  $i$ . There are three kinds of sites: central sites ( $n_i = 2$ ), bifurcation sites ( $n_i > 2$ ), and terminal sites ( $n_i = 1$ ). One has to imagine the  $1d$  tree as embedded in  $d = 3$  dimensions, each site  $i$  being surrounded by  $s_i = 6 - n_i$  walls. One considers a blind walker, which chooses with equal probability one of the six directions, being unaware of which ones are forbidden because of walls. The absorption probability is conditioned to the bouncing on the walls. The walk rules can thus be summarized in the following way: at each time step, one of the six directions is chosen with equal probability. Two possible cases arise: (i) if the chosen direction is along a branch, the walker

steps to its neighbor site; or (ii) the walker stays (bouncing on the walls) and survives with probability  $1 - \sigma$ . In any case, if the walker is not absorbed, the time counter is increased by 1 and the walk goes on; otherwise, a new walk is started. These rules have two consequences: the walkers stay longer in terminal sites, and the absorption depends on the amount of permeable surface in a coarse-grained region.

Simulations are carried for  $10^6$  walkers for values of the absorption probability  $\sigma$  ranging between  $2 \times 10^{-4}$  and  $10^{-2}$ . The average occupation number  $k_i$  is computed for each site  $i$ ,  $k_i$  being defined as the number of time steps a site has been visited by a walker. One can then define the discrete concentration  $K_i$  as the normalized occupation number:  $K_i \equiv k_i/k_0$ , where  $k_0$  is the occupation number of the entry site. Carrying further the analogy with the continuous picture, the "discrete" efficiency  $\eta_d$  of the system is defined as

$$\eta_d = \frac{\sum_i K_i s_i}{\sum_i s_i}. \quad (3)$$

To determine precisely the discrete analog of the parameter  $\Lambda$  is a nontrivial question. As  $\Lambda$  is inversely proportional to the permeability, it should be proportional to  $\sigma^{-1}$ . When plotting  $\eta_d$  directly as a function of  $\sigma^{-1}$ , the same behavior as  $\eta(\Lambda)$  is obtained (see Fig. 4). The two curves differ by only a small horizontal shift ( $\Lambda/\ell = c\sigma^{-1}$ ). This is due to the fact that  $\sigma^{-1}$  cannot be exactly identified with  $\Lambda/\ell$  in such irregular and finite treelike structures [8]. We therefore use the results from the complete PDE computation to calibrate the horizontal scale of the RW results. The factor  $c$  is found to be approximately equal to 1.3. The collapsed curves obtained by plotting the discrete efficiency versus  $(c\sigma^{-1})$  together with the curves  $\eta(\Lambda)$  from PDE computation are shown in the Fig. 4 inset. The simulations carried on the discrete topology are in very good agreement with the PDE results. This means that the behavior of the system is determined by its topological structure, geometrical details being of little importance [4]. From a practical point of view, the RW computation is more rapid and much easier to implement. On a Pentium-based PC at 1.5 GHz, the time needed to obtain a point of Fig. 4 ranges from several seconds to several minutes for the RW simulation and 2–3 h for the FEM computation.

Once validated on Kitaoka's geometries, the random walk approach can be applied to the trees determined from real human acini. Figure 5 gives the efficiency obtained for a set of eight human subacini described by Haefeli-Bleuer and Weibel [1] together with the efficiency of the  $6 \times 6 \times 6$  Kitaoka geometry. These eight subacini have somewhat different sizes, because of the anatomical variability inherent to living systems. Consequently, their responses are different. The average of the efficiencies

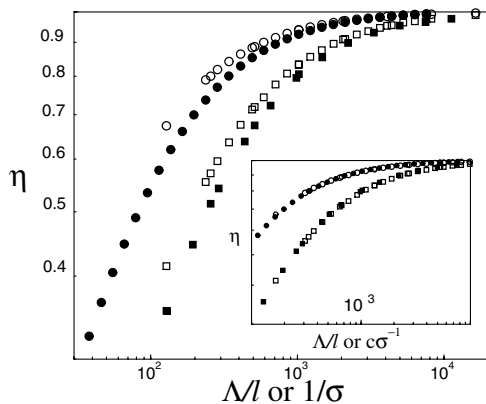


FIG. 4. Full symbols: PDE response as a function of  $\Lambda/\ell$  for  $3 \times 3 \times 3$  (circles) and  $4 \times 4 \times 4$  (squares) Kitaoka acini. Open symbols: RW calculation as a function of  $\sigma^{-1}$  for the same geometries. In the inset the same data are collapsed in a plot as a function of, respectively,  $\Lambda/\ell$  and  $c\sigma^{-1}$ , with  $c = 1.3$ .

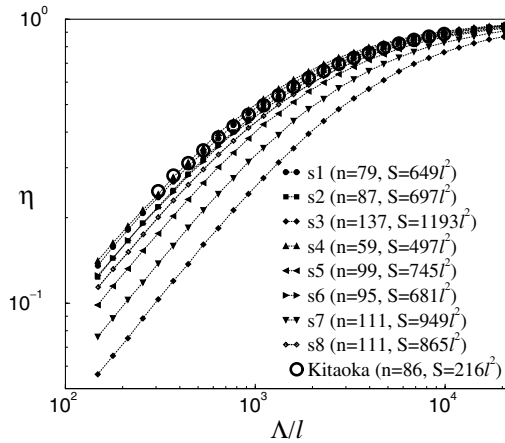


FIG. 5. Full symbol curves: discrete efficiency as a function of  $c/\sigma = \Lambda/\ell$  computed for the trees obtained from morphometric data on eight human subacini (from [1]). The big circles are obtained for the  $6 \times 6 \times 6$  Kitaoka model. The approximate area  $S$  of alveolar surface (unit length  $\ell = 0.5$  mm), and the number of branches  $n$  are indicated in the legend for each subacinus.

measured in Fig. 5 is found to be about 33%, confirming that screening is effective, at rest condition, in the human acini. At exercise condition, the increase of airflow velocity moves the source of diffusion deeper into the acinus [5]. Therefore, our results apply to a smaller sub-region of the acinus which then has an efficiency close to 1. For  $\text{CO}_2$ , screening is even stronger than for oxygen ( $\eta = 4\%$ ) because  $\Lambda$  is 20 times smaller, due to the higher membrane permeability. Nevertheless, the flux is of the same order, as it is proportional to  $\eta W$ .

In summary, it has been shown that the tools of statistical physics, such as coarse-graining procedures and discrete approaches, can be applied to the quantitative study of physiological processes in complex geometries. Whereas the complexity of the acinus geometry practically forbids computations using finite element techniques, this approach has permitted a precise estimate of the effect of diffusion screening in respiration. This physical phenomenon plays an important role in the oxygen absorption by the mammal lung, limiting its efficiency. Note that, in a reverse way, screening effects also influence the clearance of  $\text{CO}_2$  by the lung, a function equally important for respiration.

The discussion of the physiological consequences of screening goes far beyond the scope of this Letter. Let us, however, mention two facts. First, this model allows one to estimate the  $\text{O}_2$  and  $\text{CO}_2$  partial pressure differences between inspired air and blood (respectively,  $\Delta P_{\text{O}_2}$  and  $\Delta P_{\text{CO}_2}$ ). Indeed, assuming that the  $\text{O}_2$  and  $\text{CO}_2$  fluxes are equal [2], and considering Eq. (2) with  $C_0 \propto \Delta P$ , one

can write

$$\Delta P_{\text{CO}_2}/\Delta P_{\text{O}_2} = (W_{\text{O}_2}\eta_{\text{O}_2})/(W_{\text{CO}_2}\eta_{\text{CO}_2}). \quad (4)$$

Our computations give a value 2.5 for this ratio, to be compared with the experimental physiology data:  $\Delta P_{\text{O}_2}/\Delta P_{\text{CO}_2} = 110 \text{ mm Hg}/46 \text{ mm Hg} = 2.39$ . The second fact is the paradoxical observation that at constant ventilation, breathing heliox (a 20% oxygen/80% helium gas mixture) by patients in bad clinical state is more efficient than pure oxygen [9], *in spite of its lower oxygen content*. This is explained by the fact that  $\text{O}_2$  and  $\text{CO}_2$  diffusivities are greater in heliox than in air. Then, in heliox  $\Lambda$  and  $\eta$  are increased for *both* gases, whereas in pure oxygen, only the  $\text{O}_2$  uptake is increased. Furthermore, the simplicity and the rapidity of the random walk approach brings a new way to study more complex diffusion dynamics in the respiratory system. In particular, this tool should permit one to study the restricted diffusion dynamics and its relation with polarized helium MRI, in the hope to ascertain its role as a diagnostic tool for early emphysema.

The authors thank E.R. Weibel for morphological data, H. Kitaoka for providing the model acinus algorithm, and J. Soares de Andrade, Jr., T. Similowski, and C. Strauss for fruitful discussions. The Centre de Mathématiques et de leurs Applications and the Laboratoire de Physique de la Matière Condensée are C.N.R.S. “Unité Mixte de Recherches” No. 8536 and No. 7643.

- 
- [1] B. Haefeli-Bleuer and E. R. Weibel, *Anat. Rec.* **220**, 401 (1988).
  - [2] E. R. Weibel, *The Pathway for Oxygen* (Harvard University Press, Cambridge, MA, 1984).
  - [3] X. Wu, T. Nishino, and H. Liu, in *Biomedical Photonics Handbook*, edited by T. Vo-Dinh (CRC Press, Boca Raton, FL, 2003).
  - [4] M. Filoche and B. Sapoval, *Phys. Rev. Lett.* **84**, 5776 (2000).
  - [5] B. Sapoval, M. Filoche, and E. R. Weibel, *Proc. Natl. Acad. Sci. U.S.A.* **99**, 10411 (2002). In the human lung, the diffusion unit is, in fact, 1/8 of the acinus, called a subacinus by Haefeli-Bleuer and Weibel.
  - [6] M. Felici, M. Filoche, and B. Sapoval, *J. Appl. Physiol.* **94**, 2010 (2003).
  - [7] H. Kitaoka, S. Tamura, and R. Takaki, *J. Appl. Physiol.* **88**, 2260 (2000).
  - [8] Here the connectivity depends on each site coordination number, and the classical methods for solving random walks do not apply; see B. D. Hughes, *Random Walks and Random Environments* (Clarendon Press, Oxford, 1995).
  - [9] E. M. Schaeffer, A. Pohlman, S. Morgan, and J. B. Hall, *Crit. Care Med.* **27**, 2666 (1999).